J. Water Environ. Nanotechnol., 7(1): 31-43 Winter 2022

ORIGINAL RESEARCH PAPER

Cathodic synthesis of Al-Ce-Mn Oxide nanohybride powder with improved surface for effective removal of fluoride from aqueous media

Abbas Ariamanesh[1], Ramin Yavari[2], Taher Yousefi [2*], Dariush Rezaei Ochbelagh [1]

[1] Departments of Nuclear Engineering and Physics Amirkabir University of Technology Tehran Iran
[2] Nuclear Fuel Cycle Research School, Nuclear Science and Technology Research Institute, Tehran, Iran

Received: 2021-9-14 Accepted: 2021-12-20 Published: 2022-02-01

ABSTRACT

Al-Ce-Mn oxide samples were synthesized by the cathodic electrochemical method at current densities of 5, 15, and 35 $mAcm^{-2}$. The XRD, SEM, and EDX techniques were used for the characterization of samples. The SEM images show that at high current density the one-dimensional(nanowire) structure and at low current density two-dimensional (nanosheet) structure were obtained. Moreover, the particle sizes are decreased with increasing the current density. The samples were applied for the uptake of fluorine (F^-) ions from solutions. The influence of the contact time, initial fluoride concentration, and solution pH on the adsorption was investigated. The results showed more than 80 % of F- ions were uptake from solution during the three hours initial contact times and the uptake capacity has little change at pH below 6 and it has a sharp decline with increasing solution pH. The kinetic data were well fitted to the pseudo-second-order model and the equilibrium adsorption data was well described by the Langmuir isotherm model. The adsorption capacity was 48 mg/g at pH 6 and room temperature.

Keywords: *Al-Mn-Ce Oxide, Adsorption, Fluoride, Nanowire, Electrodeposition*

How to cite this article
FAMILY N. Cathodic synthesis of Al-Ce-Mn Oxide nanohybride powder with improved surface for effective removal of fluoride from aqueous media. J. Water Environ. Nanotechnol., 2022; 7(1): 31-43.
DOI: 10.22090/jwent.2022.01.003

INTRODUCTION

Small anionic radius, high affinity to act as a ligand, and the formation of a great number of various organic and inorganic compounds are characteristics of fluoride (F^-) ions**.** The fluoride (F^-) ions are present in various inorganic and organic materials in soil, rocks, air, plants, and animal bodies.

The high solubility (in water) of the fluoride compounds would lead to the production of dissociated fluoride ions in groundwater and surface [1-4]. Two main sources of fluoride (F^-) ions in groundwater and on the surface as anionic contaminants are geochemical reactions and disposal of industrial wastewaters [1-4].

The industrial activities which lead to producing fluoride contaminated wastewater originate form are glass and ceramic productions, electroplating, semiconductor manufacturing, coal-fired power stations, beryllium extraction, brick and ironworks, and aluminum smelters [5]. Human and other creatures' health can be affected by the pollution of groundwater with fluoride ions.

An excess intake of fluoride is harmful to our health; for instance, it can cause dental/skeletal fluorosis [6-8].

As an unwanted hazardous intake, the presence of fluoride ions over the threshold concentration of 1.5 mg/L in water can be harmful [9]. The studies showed that drinking water is the primary source of daily intake of the fluoride ions and consumption of drinking water with high fluoride concentrations for a long time can induce various

* Corresponding Author Email: *taher_yosefy@yahoo.com*

defects in birth, reproduction, immunological and anatomical problems including dental and skeletal fluorosis [10]. Therefore the removal of fluoride (F^-) ions from drinking water and wastewater are very vital and important[11]. Different chemical and physical treatment methods have been used for the uptake of fluoride from wastewater. These methods are coagulation[12], precipitation, surface adsorption [11], ion exchange, and membrane processes (Nano-filtration, Reverse osmosis) [14] and electrolytic treatment [11, 15-18].Among these methods, adsorption is found to be the most commonly used and popular method arising out of its simple operation, low cost, and highly efficient technique [13-19]. Various natural and synthesized adsorbents have been used for the removal of fluoride ions from water[20]. Natural materials such as zeolites, clays, and chitosans are inexpensive, green, and available adsorbents, but the low capacity has limited their usage in fluoride removal. The problem of natural adsorbents (low capacity) can be tackled by modification of natural adsorbents or utilization of synthesized materials. In recent years, several rare and transition metal oxides such as zirconium oxide, titanium oxide, cerium oxide, and iron(III) oxide have been used for the treatment of wastewater to eliminated fluoride ions treatment [21-22]. The high adsorption capacities and environmental friendliness are the attractive properties of these metal oxides as adsorbents for the uptake of fluoride ions from wastewater. Also, the results cleared that the multimetal oxides have higher fluoride uptake capacity, especially when the rare metals are present as multimetal oxides [21-22]. The main reasons for the high fluoride (F^-) removal capacity of the metal/multimetal oxides can be described by the modification of the net charge of metal/multimetal oxide surface that facilitates the removal of fluoride through physisorption [21-22].

More recent investigations revealed that rare-earth elements, such as Lanthanum and Cerium when associated with other metals forming composite materials, such as Al-Fe-La [23], Fe-Mg-La [24], Fe-La, Fe-La-Ce[25], Ca-Al-La [26], Mg-Ce-La [27], Fe-Al-Ce [28], Zr-Al-La [29] develop a high affinity to fluoride. It is known that the synergistic interactions of metals promote an improvement in the adsorptive capacity of materials for fluoride[11]. As compared to Cerium, Mn oxide is considered a low-cost material, and its composites also have good adsorption capacity for fluoride [11, 29], as well as aluminum oxide. So, mixing rare earth metals (La, Ce) with low-cost metals (Al, Mn) could be advantageous to achieve high adsorption capacities at a neutral pH solution.

Also, the adsorbent material's fluoride removal performance can be associated with the synergistic effect of some properties such as structure, porosity, and Ce-Al-Mn interactions in the surface material.

Thus the mixed valance of metals in multimetal oxide have an additional net charge on their surface compared with the single metal oxides and the additional surface charge induces a stronger van der Waals attraction force for the adsorption of ions resulting in higher ion uptake capacity. In the current work Ce–Mn–Al tri-metal composite oxide was synthesized by the electrochemical methods and its potentials as an adsorbent for adsorption of fluoride and treatment of fluoride contaminated water were assessed thorough investigation of the effect of influencing factors such as time, initial concentration and pH. The adsorbents were characterized by X-ray Diffraction (XRD), Scanning Electron Microscopy (SEM), and the Fourier transform infrared spectroscopy (FTIR).

EXPERIMENTAL

Chemicals and reagents

The materials; $Mn(NO_3)_2 4H_2O$, $Al(NO_3)_3 9H_2O$, $NaNO_3$, $Ce(NO_3)_3 6H_2O$ HNO_3, NaOH, and TIZAB (Trans-1,2-Diaminocyclohexane-N,N,N′,N′-tetraacetic acid monohydrate) purchased from Merck (Germany), were utilized without further purification. The solutions were prepared from distilled water. The working electrode (cathode) was made up of stainless steel plates (316 L, 5×12×0.5 mm), placed between the two-rod graphite electrodes acting as anodes. The current densities of 5, 15, and 35 mA cm^{-2} were applied for deposition at different periods**.**

Preparation of adsorbent (Ce-Mn-Al tri-metal) and fluoride measurement.

The Al-Mn-Ce nano oxide was deposited at current densities of 5, 15, and 35 $mAcm^{-2}$. The main reactions at work electrode (cathodic reactions) for metal deposition were OH^- electro-generation reactions or dissolved oxygen, water, and nitrate ions reductions reactions as follows [30-34].

$$2H_2O + 2e^- \rightarrow H_2 + 2OH^- \quad (1)$$

$$O_2 + 2H_2O + 4e^- \rightarrow 4OH^- \quad (2)$$

$$O_2 + 2H_2O + 2e^- \rightarrow 2OH^- + H_2O_2 \quad (3)$$

$$NO_3^- + H_2O + 2e^- \rightarrow NO_2^- + 2OH^- \quad (4)$$

These reactions led to the production of OH^- ions, increasing the local pH and deposition of Mn-Ce-Al hydroxide at the cathode surface as:

$$Mn(II) + Al(III) + Ce(III) + xOH^- \rightarrow Mn - Al - Ce - (OH)_x \quad (5)$$

Just after the completion of the reaction, the Mn-Ce-Al-$(OH)_x$ powder was stripped from the electrode surface. The mixed hydroxide was then converted to an oxide by heat treatment:

$$Mn - Ce - Al - (OH)_x \xrightarrow{\Delta, 1000^\circ C} Mn - Ce - Al - (OOH)_x A \rightarrow Mn - Ce - Al - O_x \quad (6)$$

The F^- ions adsorption experiments were conducted in the batch mode and the effects of influencing parameters such as initial concentration, pH, and time were investigated. The stock fluoride (F^-) solution was prepared by dissolving an appropriate amount of NaF in distilled water. 0.05 mg of the Mn-Ce-Al-$(OH)_x$ powder was poured into a specified volume of F^- aqueous solution, and stirred in a temperature-controlled shaker. The stirring speed of 400 rpm was chosen for all the experiments

characterization

The products were characterized by X-ray diffraction pattern STOE STADI MP diffractometer equipped with monochromatized CuK_α radiation (k = 0.154 nm, 40 kV], Scanning Electron Microscopy (SEM, model EM-3200 China). The fluoride concentrations were determined by a Metteler Toledo Seven Compact S220 pH/Ion meter (Switzerland) equipped with an ISTEK fluoride ion-selective electrode.

RESULTS AND DISCUSSIONS

Characterizations

Morphology

Fig. 2 shows the SEM images of the Mn-Ce-Al composites prepared at different current densities of 5, 15, and 35 $mAcm^{-2}$. Based on the figure, the surface morphologies show significant changes when the current density varied from 5 to 35 $mAcm^{-2}$. At a high current density of 35 $mAcm^{-2}$, the one-dimensional structure (nanowire with an average diameter of 50nm) is produced, whereas the decrease in the current density leads to the disappearance of the nanowire and appearance of the nanosheet structures. Moreover, the particle sizes are decreased with increasing the current density and turning to a smooth wire shape structure. Energy dispersive X-ray (EDX) spectroscopy results of the synthesized samples at different current densities are shown in Fig.1d. As seen, the Al, Mn, and Ce elements are not the same in all samples. The Mn content increases by increasing the current density.

Based on Ksp values as:

$$Al^{3+} + 3OH^- \rightarrow Al(OH)_3$$
$$K = [Ksp_{Al(OH)_3}]^{-1} = 3.33 \times 10^{33} \quad (7)$$

$$Mn^{2+} + 2OH^- \rightarrow Mn(OH)_2$$
$$K = [Ksp_{Mn(OH)_2}]^{-1} = 2.5 \times 10^{12} \quad (8)$$

$$Ce^{3+} + 3OH^- \rightarrow Ce(OH)_3$$
$$K = [Ksp_{Ce(OH)_3}]^{-1} = 5 \times 10^{19} \quad (9)$$

OH^- generation at electrode surface leads to the formation of $Mn(OH)_2$, $Ce(OH)_3$, and $Al(OH)_3$, respectively. Also, it is well known that the MnO_2 structures are one-dimensional (rod, wire). In other words, the crystal growth mechanism of MnO_2 is anisotropic growth. The chemical potential of the MnO_2 in solution and inherent structure of the MnO_2 material tend to anisotropic growth mechanism in particles formation. In the first step, due to the high surface energies of the initial synthesis nuclei, the accumulation takes place and spherical nanoparticles form (Ostwald Ripening). Then, the spherical nanoparticles would gradually transform into a one-dimensional structure (wire or rod). The gradual conversion of the nanoparticles into the one-dimensional structure (wire or rod) can be attributed to their anisotropic nature and the preferential one-dimensional growth of Mn components. In other words, from the thermodynamic and kinetic points, the crystal growth of Mn components in one axis is prevailed entailing one-dimensional structures. Thanks to literature, we can easily find that the common structures of manganese hydroxide/oxide are one-dimensional [32,34].

At high current density (of 35 $mAcm^{-2}$),

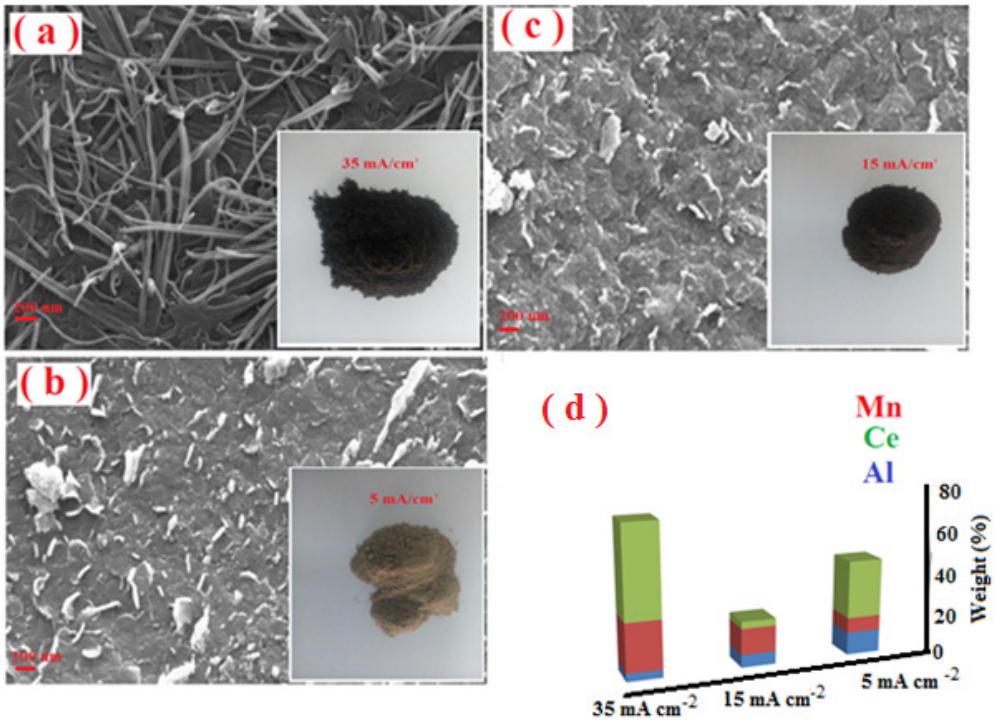

Fig. 1, SEM images of synthesized samples at (a) 35, (b) 15 and (c) 5 mAcm^{-2}current density. (d) Results of Energy dispersive X-ray (EDX) spectroscopy

because of the high OH^- concentration generation in the initial step of the electrosynthesis and based on $K_{SP\ (Mn(OH)2}$, the Mn value in the deposit is high (as it was approved by EDS results). So, $Mn(OH)_2$ has a primary and significant role in the structure formation, and the structure of the product is conducted by the anisotropic nature of Mn; consequently, the nanowire is produced. As current density decreases, the amount of the Mn hydroxide in the deposit is decreased (see the EDS result) and the amounts of Ce and Al which tend to be irregular and three-dimensional are increased in the deposit thus, the crystal growth does not follow the anisotropic process. As a result, the crystal growth diverts from the one-dimensional to the three-dimensional mechanism. In the following items some of the major nanostructure mechanisms formations will be discussed:

Growth control by surfactant and additives

The crystal shape and morphology of the metal oxide result from the different crystal growth rates in various directions because the surface energy levels are not the same in different planes of the crystal. The high-index planes usually have higher surface energy. However, the exact mechanism for the formation of these architectures has not been fully understood [35].

Thus, faster growth along the special direction can lead to the phenomenon of special morphology (particles, wire, tube, rod, etc.). To get various morphologies necessitates the control of the growth rate of different facets of the nuclei [36-37]. For this purpose, surfactant, templates, or other specific assets are applied. For example, the NH_3 molecules in solution can form an ordinate bond with the M ions on the surface; so, they can cancel the crystal growth. The density of the adsorbed NH_3 depends on the density of the metal ions on the crystal plane. The densities of the metal ions in the crystal planes are not the same. For example, in the CuO crystal the order of Cu ions in the crystal is as: (001) > (100) > (010) (Li et al, 2008). In the solution with the initial concentration of Cu^{2+} and high NH_3 concentration, all primary CuO nuclei planes are coordinated, resulting in a weak driving force for further aggregation and 1D, 2D, and 3D nanoplates formation. With an increase in Cu^{2+} concentration, the growth in 010 would be dominant because NH_3 is bonded to Cu ions in 001 and 100 planes, slowing down the crystal growth in these directions, while the growth in the 010 direction would be faster

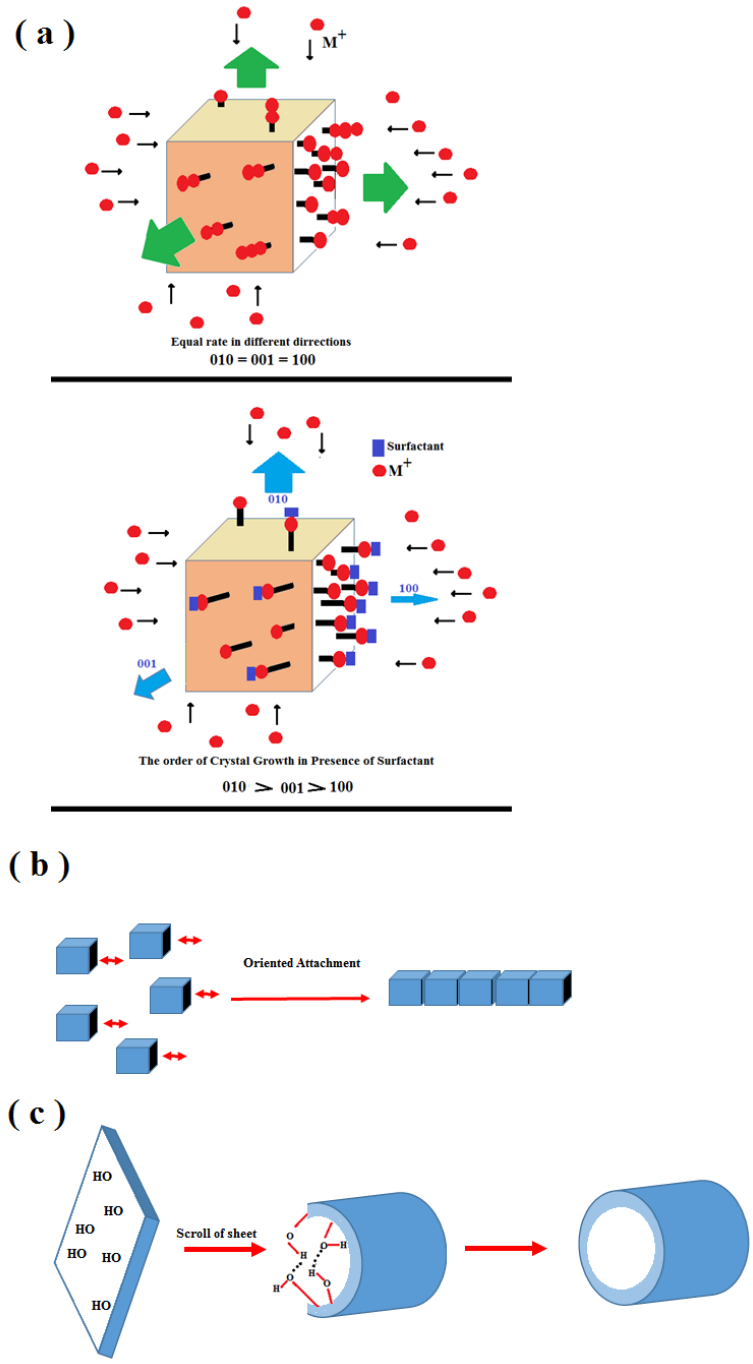

Fig. 2, (a) Growth control by Surfactant and additives, (b) Oriented attachment, and (c) Scroll of sheets crystal growth mechanisms

resulting in the nanorods or nanowires (Fig.2a) (Li et al, 2008). The non-identical density of Mn^{2+} ions in the crystal planes of as-prepared $Mn(OH)_2$ is responsible for faster growth of particles in a direction and 1D nanostructure formation.

Oriented attachment [38]

Oriented attachment is a crystal growth mechanism in which the attachment of the small crystallites on suitable planes or facets along the same directions occurs. In the oriented attachment,

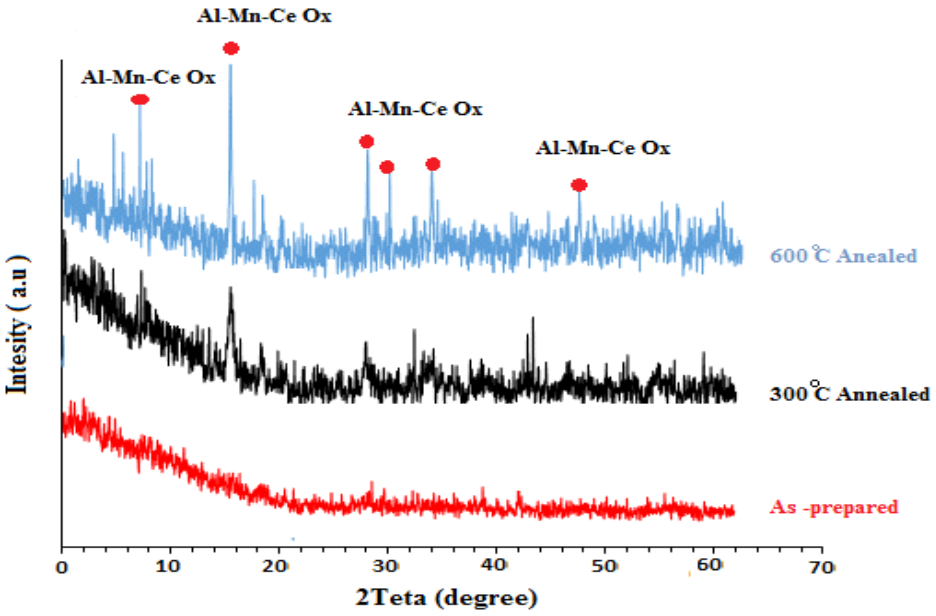

Fig. 3, XRD pattern of as-prepared and temperature annealed (300 and 600 ˚C) samples

large particles could be formed in an irreversible and highly oriented manner. Commonly, the particle or sphere and or any other irregular shape structures (the result of crystal growth in three dimensions), would be resulted. However, the control of the crystal growth in the special direction by a surfactant, capping agent, etc. is possible (Fig.2b).

Scrolling of sheets

In as-prepared $M(OH)_2$, the dangling OH groups in the layer edges under certain conditions, link together (hydrogen bond interactions). As a consequence, the edges can be connected and the sheets roll to form $M(OH)_2$ tubular form [39] (Fig.2c).

XRD

The XRD patterns of as-prepared and temperature annealed (300 and 600 ˚C) samples are shown in Fig.3. As can be seen, an as-prepared sample has an amorphous structure, since no signs of crystalline phase can be seen in the pattern. While the heat-treated samples show clear and sharp peaks related to Al-Mn-Ce oxide, indicating an improvement most in the crystal quality of the nanostructures. Also, the results show that the intensities of the peaks were improved with the temperature increasing.

Adsorption

Adsorption experiments were carried out using a batch method. In order to determine the F^-adsorption capacity of Al-Mn-Ce oxide samples synthesized at different current densities, 0.05 g of the adsorbents was added to 20 ml of NaF solutions with concentrations of 25mgL^{-1} (Fig.4). The samples were shaken at 400 rpm and 25°C for 24 hours. After shaking, the sorbent from the solution was separated by filtration and the concentration of fluoride ions was measured by an F^- selective electrode. The sorption capacity of the samples was evaluated according to the following expression [40-41]:

$$q_e = (C_i - C_e)\frac{v}{w} \quad (10)$$

where q_e (mg g^{-1}) is the amount of F^- ions removed per unit mass of an adsorbent, C_i and C_e (mg L^{-1}) are F^- ions concentrations in the liquid phase at t=0 and t=t_e respectively, V (L) is the volume of suspensions and w (g) is the mass of the adsorbent. The results show that the samples have approximately the same F^- adsorption capacity and sample 1 (synthesized at 35 mA cm^{-2}) has a slightly higher capacity. Therefore, sample 1 with nanowire morphology was selected for further studies.

In order to evaluate the adsorption kinetic, 0.05 g of sample 1 was suspended in20 ml of 25 mg

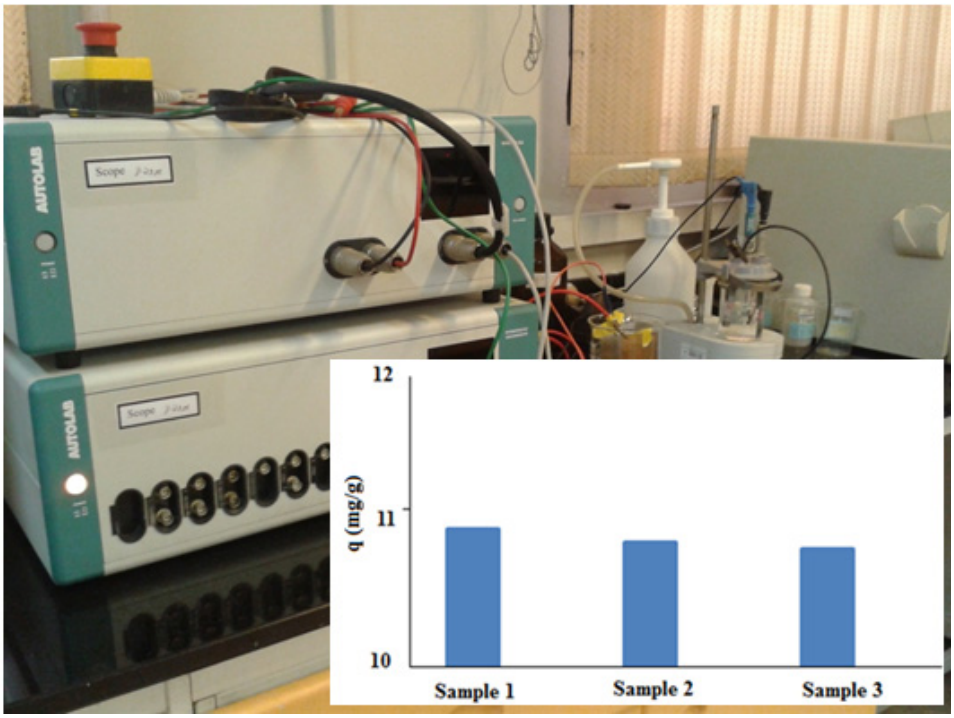

Fig. 4. Adsorption capacity of: sample1= 35 mA cm^{-2}, sample2= 15 mA cm^{-2}, sample 3= 5 mA cm^{-2}

g^{-1} NaF solution at 25 °C and 400 rpm for various intervals time ranging from 15 minutes to 24 h (Fig. 5).

Fig. 5 depicts the variation of qt (mg g^{-1}) versus the contact time (h) of the F^- adsorption by Al-Mn-Ce Oxide. The results indicated that the uptake of F- ions was quite rapid and the requested time (min) for achieving the highest capacity was about 200 min. In other words, more than 80 % of F^- ions were uptake from the solution during the three hours initial contact times. The fitting of experimental data with two important kinetic models of pseudo-second-order and pseudo-first-order models shows that the pseudo-second-order is more in agreement with the obtained data compared with the pseudo-first-order model. The pseudo-first-order and pseudo-second-order kinetic models are given in Equations 11 and 12, respectively [40-41].

$$\frac{dq_t}{d_t} = K_I\left(q_e - q_t\right) \quad (11)$$

$$\frac{dq_t}{d_t} = K_{II}(q_e - q_t)^2 \quad (12)$$

Where, q_e and q_t are the sorption capacity (mg/g) in equilibrium state and time t, respectively. The K_I and K_{II} are kinetic rate constants. In the pseudo-second-order model, the availability of the active sites on the sorbent for ions (sorbates) is regarded as the overall sorption rate-limiting factor. In other words, the uptake capacity of the sorbent is proportional to its occupied active sites number [42-43].

To find the effect of the initial concentration on the fluoride removal, 0.05 g of adsorbent was added to the 20 ml of NaF solution with the concentration of 25, 125, 250, and 500 mg g^{-1}. The suspensions were shaken at 400 rpm for 24 h at 25 to 60 °C (Fig. 6.). The results indicated that the uptake of fluoride by the composite is first increased and then become constant with increasing the F- concentration. The maximum sorption capacity of 48 mg/g was found at 500 mg L^{-1} initial concentration which reflects the high ability of the synthesized composite for F^-ions adsorption compared with the reported materials (Table 2).

Adsorption Mechanism and effect of solution pH

The adsorption mechanism of F^- by the metal oxides is complicated. Based on the chemical composition, the functional groups of Al-Mn-Ce Oxide, and reports [62] the adsorption mechanism

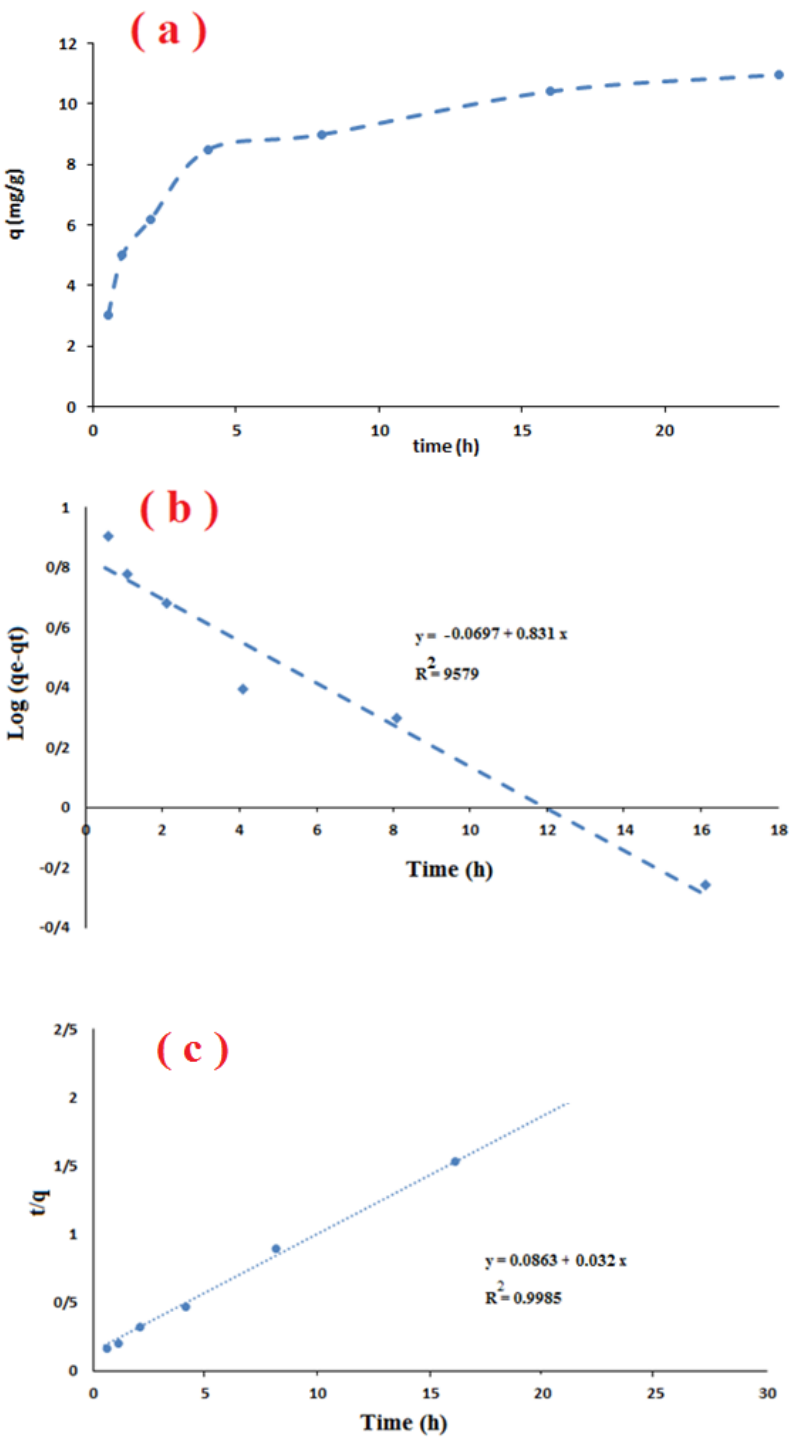

Fig. 5, (a) The plot of q_e versus t(h) of F^- adsorption on Al-Mn-Ce oxide (Ci=25.0 mg g^{-1}, T= 298 K), (b) Pseudo first-order kinetic model, (c) Pseudo second-order kinetics fit for F- sorption

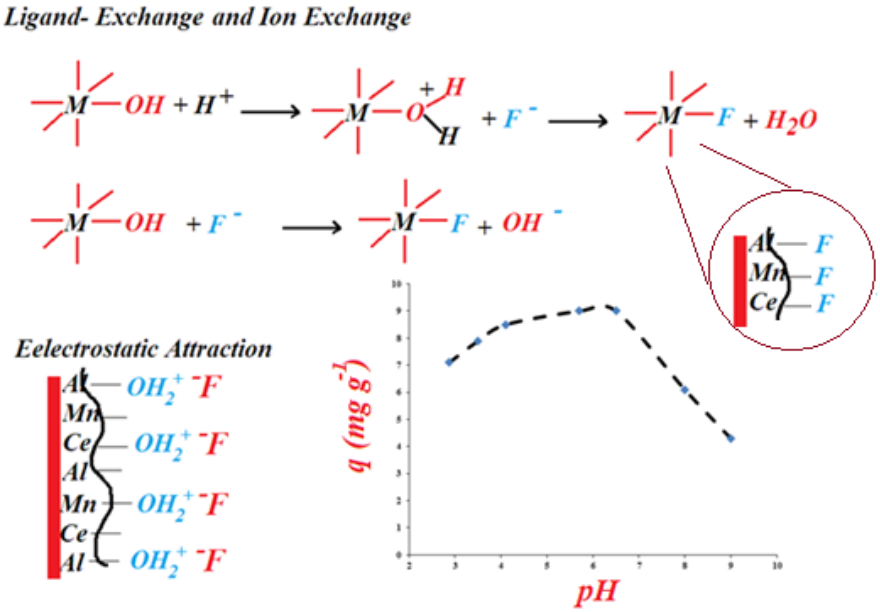

Fig. 6, F- adsorption mechanism and effect of pH on adsorption capacity

Table 1, Kinetic parameters of pseudo-first-order and pseudo-second-order kinetic models.

	K_I or K_{II}	q_{max}	R^2
Pseudo first-order	0.831	1.7	0.9579
Pseudo second-order	0.007	31.25	0.9985

can be proposed in order to determine the potential application of the obtained adsorbent.

The net surface charge, due to the defects of lattice, and the surface hydroxyl groups [62] on Al-Mn-Ce Oxide are the active adsorption agents for the uptake (adsorption) of F^- in solution, by the electrostatic interaction and ion-exchange (ligand or ion-exchange with the fluoride ions) following the equations. Due to the similarity of OH^- and F^- ionic radii and the higher coordination ability of F^- compared with OH^-, the coordination of Al-Ce-Mn oxide with $F^-$is better than that of OH^- (strong chemical bond with metal), therefore, the ligand-exchange would happen [62]. Based on the EDX results the sample with a greater Ce value (the sample obtained at 35 mA cm^{-2}) showed higher adsorption capacity, hence it seems that the Ce–OH was the preferential adsorption site for the fluorine (F^-) adsorption by the ligand exchange mechanism. However, the role of Al_3-OH and Mn_3-OH with higher positive charges in fluorine (F^-) adsorption by electrostatic attraction cannot be ignored. In the same condition, the pure oxide of MnO_2, Al_2O_3, and CeO_3 was synthesized and their fluorine (F^-) adsorption capacity was evaluated. The results showed that the adsorption capacities of MnO_2, Al_2O_3, and CeO_3 are less than 15 mg g^{-1}. This result cleared that the synergistic interaction between Al, Ce, and Mn in the Al-Ce-Mn composite makes the special and favorite structure a desirable surface with a high active adsorption site for the fluoride adsorption. In other words, the multivalent cations such as La^{3+}, $Ce^{3+,}$ and Zr^{4+} dramatically change the surface properties of the composites and their affinity for fluoride. Since these metals are expensive, preferably, some cheaper metals such as Al, Fe, Mn, etc. are mixed with these metals to prepare the hybrid adsorbents.

In the adsorption, process pH is considered as an important factor that affects the adsorbent surface and sorbate ions as well as the competitor's behavior in solution. The pH effect on F^- adsorption was studied in 25 mg g^{-1} NaF solution at 25 °C by adjusting the solution pH with the NaOH or HNO_3. As can be seen, the uptake capacity has little change at pH below 6 and it has a sharp

Table 2. Comparison of adsorption capacity of some adsorbents for fluoride.

No	Adsorbent	q_{Max}(mg m^{-1})	Year	Reference
1	Nano-hydroxyapatite/stilbite composite	9.15	2016	[44]
2	Bone Char	1.08	2017	[45]
3	Cerium-containing Bone Char	13.60	2017	[45]

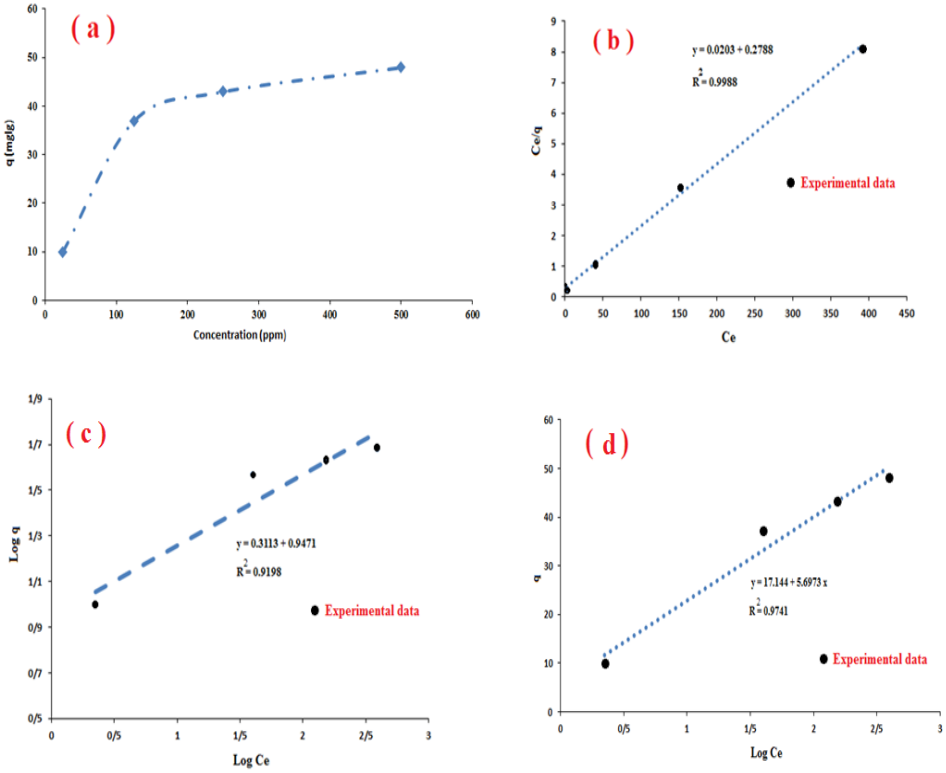

Fig. 7, (a) Effect of initial ion concentration (25, 125, 250, 500 mgL^{-1}) on adsorption of F^- at 298K, (b) The linearized Langmuir, (c) The linearized Freundlich, (d)linearized Temkin isotherms for adsorption of F^- Al-Mn-Ce Oxide.

decline with increasing solution pH. Based on the ligand exchange mechanism (Fig.6) in an acidic solution as a result of the protonation of hydroxyl groups convert them into good leaving groups for substitution viz. exchange of the F- ions. Also, in a low solution pH, the surface positive net charge of Al-Mn-Ce Oxide increases. Based on the electrostatic attraction mechanism, it leads to a stronger attraction of the F- ions and an increase in the adsorption capacity, in the long run. The F^- uptake capacity is decreased with further increasing the pH values (>6) which can be attributed to the competition between hydroxyl and fluoride ions for the active adsorption sites and decreasing of positive net charge of Al-Mn-Ce surface at a high pH [63].

The F^- adsorption was described by Langmuir, Freundlich, and Temkin, isotherm models (Fig. 8).

Linear expression of Langmuir adsorption isotherm is as follows (Eq.13

$$C_e/q_e = 1/bK + C_e/b \quad (13)$$

where q_e is the uptake capacity (mg g^{-1}), Ce is the F equilibrium concentration (mg L^{-1}),

and K (L mg^{-1}) and b are the Langmuir constants related to the uptake capacity and adsorption energy respectively [30].

In the Freundlich isotherm model, the sorption mechanism is based on the multilayer location of the species on a heterogeneous surface with variable binding energy [64]. The Freundlich expression is

Table 3 Calculated Langmuir constants

q_e	C_e	q_m	K_L
9 (mg/g)	2.5 ppm	50.86 (mg/g)	0.823
37 (mg/g)	32.5 ppm	50.23 (mg/g)	0.263
43 (mg/g)	142.5 ppm	46.50 (mg/g)	0.075
48 (mg/g)	380 ppm	49.46 (mg/g)	0.029

as follows:

$$Ln(q_e) = Ln(K_F) + \left(\frac{1}{n}\right) Ln(C_e) \quad (14)$$

where q_e(mg g^{-1}) is the uptake capacity, C_e(mg L^{-1}) is the F^- equilibrium concentration, K_F (mg/g) and 1/n are Freundlich describing the quantity and quality of the adsorption, respectively.

The Temkin isotherm is based on the interactions between the sorbent and sorbate and linear decrease of the sorption heat of ions in the layer (than logarithmically) [64-66]. The model is expressed as:

$$qe = RT/b\ Ln(ATCe) \quad (15)$$
$$B = RT/b_T$$
$$q_e = BLnA_T + BLn\ C_e \ldots\ldots.$$

where A_T (L/g) is the equilibrium binding constant, b_T is the Temkin isotherm constant, R(8.314J/mol/K) is the gas constant, T(K) is the temperature, B (J/mol) is a constant related to the sorption heat.

The results of the modeling with linearized Langmuir, Freundlich, Temkin models and their correlation coefficients are shown in Fig. 7. The correlation coefficient results show that the Langmuir model fitted the experimental data better than the others. The isotherm parameters for the Langmuir plot are given in Table 3. The maximum sorption capacity (q_{max}) of the Al–Mn-Ce estimated from the Langmuir model was 49.53 mg g^{-1} at 25 °C which was compatible with the experimental result (48 mg g^{-1}).

CONCLUSION

Al-Mn-Ce oxide was synthesized for the first time through the electrochemical base generation method at three different current densities(5, 15, and 35 $mAcm^{-2}$). The samples were characterized by XRD, SEM, and EDX techniques. The results indicated the chemical composition, uptake capacity, and morphology changes of samples with varying current densities. Three nanostructure mechanisms of the formation such as Growth control by surfactant and additives, Oriented attachment, and Scrolling of sheets were discussed. The adsorption of fluoride ions from an aqueous solution by the synthetic Al-Mn-Ce oxide was studied under different experimental conditions such as time, pH, and initial concentration. In the same condition, the pure oxide of MnO_2, Al_2O_3, and CeO_3 was synthesized and their fluorine (F^-) adsorption capacity was evaluated. The results showed that the adsorption capacities of MnO_2, Al_2O_3, and CeO_3 are less than 15 mg g^{-1}. The synthesized Al-Mn-Ce Oxide nanowire (synthesized at 35 mA cm^{-2}) exhibited a high defluoridation capacity of 48 mg g^{-1}. The adsorption mechanisms were conducted through the electrostatic attraction, as well as the ionic exchange/ligand exchange process. The hydroxyl groups and positive net charge due to the defect in the crystal structure of the Al-Mn-Ce oxide surface play important roles in the adsorption process. The F^- adsorption kinetics and isotherms follow Langmuir and pseudo-second-order models, respectively. The findings revealed that Al-Mn-Ce oxide nanowire is a promising material for the removal of fluoride ions in relatively short contact time and a wide pH range.

CONFLICTS OF INTEREST

There are no conflicts to declare.

REFERENCES

[1] Saxena VK, Ahmed S. Dissolution of fluoride in groundwater, Environ.Geol. 2001; 40:1084–1087.
[2] Tor A. Removal of fluoride from an aqueous solution by using montmorillonite, Desalination, 2006; 201: 267–276.
[3] Daifullah AAM, Yakout SM, Elreefy SA. Adsorption of fluoride in aqueous solutions using $KMnO_4$-modified activated carbon derived from steam pyrolysis of rice straw, J. Hazard. Mater. 2007;147:633–643.
[4] Sun Y, Fang, Q, Dong J, Cheng X, Xu J. Removal of fluoride from drinking water by natural stilbite zeolite modified with Fe(III), Desalination, 2011; 277: 121–127.
[5] Shen F, Chen X, Gao P, Chen G. Electrochemical removal of fluoride ions from industrial wastewater, Chem. Eng. Sci.,

2003;58: 987–993.
[6] Jiabin C, Renjie Y, Zhiyong Z, Deyi W. Removal of fluoride from water using aluminum hydroxide-loaded zeolite synthesized from coal fly ash, Journal of Hazardous Materials. 2022; 421: 126817.
[7] Hao D, Huan T, Xinxing S, Wenlan Y, Wenjing C, Han L, Yu Z, Zhengyong Z, Ming H. Enhanced fluoride removal from water by nanosized cerium oxides impregnated porous polystyrene anion exchanger, Chemosphere 2022; 287:131932.
[8] Umma S, Rashid, Tonoy KD, Tamil SS, Sudipta S, Achintya NB. GO-CeO_2 nanohybrid for ultra-rapid fluoride removal from drinking water, Science of the Total Environment, 2021; 793: 148547.
[9] Geneva, World Health Organization, Guidelines for Drinking-Water Quality: Incorporating First Addendum Recommendations, vol. 1, 3rd ed., World Health Organization, 20 Avenue Appia, 1211, Switzerland, 2006;1 : 375–376.
[10] Habuda SM, Ravančić ME, Flanagan A. A Review on Adsorption of Fluoride from Aqueous Solution, Materials, 2014; 7: 6317-6366.
[11] Juliana MG, Davi R, André Luis de O, Perilli Dison SP, Franco Elvis C, Edson Luiz F, Sergio L, Jahn Guilherme LD. A novel Fe-Al-La trioxide composite: synthesis, characterization, and application for fluoride ions removal from the water supply, Journal of Environmental Chemical Engineering, 2021; 9:106350.
[12] Neeraj C, Parmesh Kumar C, Ghoshna J, Abhinesh P, Raghwendra Singh T. Removal of fluoride from water by electrocoagulation using Mild Steel electrode, Journal of the Indian Chemical Society 2021; 98:100026.
[13] Shraban K, Sahoo GH. Surface functionalization of GO with MgO/$MgFe_2O_4$ binary oxides: A novel magnetic nanoadsorbent for removal of fluoride ions, Journal of Environmental Chemical Engineering, 2018; 6 :2918–2931.
[14] Zhu J, Zhao HZ, Ni JR, Fluoride distribution in electro coagulation defluoridation process, Sep. Purif. Technol. 2007; 56: 184–191.
[15] Mourabet M, ElRhilassi A, ElBoujaady H, Bennani ZM, ElHamri R, Taitai A. Removal of fluoride from aqueous 266 solution by adsorption on Apatitic tricalcium phosphate using Box–Behnken design and desirability function, Appl. Surf. Sci., 2012; 258: 4402–4410.
[16] Wang SG, Ma Y, Shi YJ, Gong WX. Defluoridation performance and mechanism of nano-scale aluminum oxide hydroxide in aqueous solution, J. Chem. Technol. Biotechnol. 2009; 84: 1043–1050.
[17] Meenakshi S, Viswanathan N. Identification of selective ion-exchange resin for fluoride sorption, J. Colloid Interface Sci. 2007; 308:438–450.
[18] Arora M,Maheshwari RC, Jain SK, Gupta A. Use of membrane technology for potable water production, Desalination, 2004;170:105–112.
[19] Fan X, Parker DJ, Smith MD. Adsorption kinetics of fluoride on low cost materials, Water Res. 2003; 37:4929–4937.
[20] Yu Y, Yu L, Paul JC. Adsorption of fluoride by Fe–Mg–La triple-metal composite: Adsorbent preparation, illustration of performance and study of mechanisms, Chem. Eng. J., 2015; 262:839–846.
[21] Dou X, Zhang Y, Wang H, Wang T, Wang Y. Performance of granular zirconium–iron oxide in the removal of fluoride from drinking water, Water Res. 2011; 45: 3571–3578.
[22] Chen L, He BY, He S, Wang TJ, Su CL, Jin, Y. Fe–Ti oxide nano-adsorbent synthesized by co-precipitation for fluoride removal from drinking water and its adsorption mechanism, Powder Technol. 2012; 227: 3–8.
[23] Adak MK, Sen A, Mukherjee A. Removal of fluoride from drinking water using highly efficient nano-adsorbent, Al(III)-Fe(III)-La(III) trimetallic oxide prepared by chemical route. J Alloys Compd. 2017; 719:460–469.
[24] Yu Y, Yu L, Paul Chen J. Adsorption of fluoride by Fe-Mg-La triple-metal composite: Adsorbent preparation, illustration of performance and study of mechanisms. Chem Eng J 2015; 262:839–846.
[25] Thathsara SKT, Cooray PLAT, Mudiyanselage TK. A novel Fe-La-Ce tri-metallic composite for the removal of fluoride ions from aqueous media. J Environ Manage. 2018; 207:387–395.
[26] Xiang W, Zhang G, Zhang Y. Synthesis and characterization of cottonlike Ca-Al-La composite as an adsorbent for fluoride removal. Chem Eng J. 2014; 250:423–430.
[27] Zhang C, Li Y, Wang TJ. Adsorption of drinking water fluoride on a micron-sized magnetic Fe_3O_4 @Fe-Ti composite adsorbent. Appl Surf Sci. 2016; 363:507–515.
[28] Zhao B, Zhang Y, Dou X, Granulation of Fe-Al-Ce trimetal hydroxide as a fluoride adsorbent using the extrusion method. Chem Eng J, 2012; 185–186: 211–218.
[29] Zhou J, Zhu W, Yu J. Highly selective and efficient removal of fluoride from ground water by layered Al-Zr-La Tri-metal hydroxide. Appl Surf Sci. 2018; 435: 920–927.
[30] Moazami HR, Davarani HS, Yousefi T, Keshtkar AR. Synthesis of manganese dioxide nanosheets and charge storage evaluation, Mater. Sci. Semicond. Process. 2015; 30: 682-687.
[31] Yousefi T, Nozad GA, Mashhadizadeh MH. Synthesis and characterization of cerium oxide nano-particles in chloride bath: effect of the H_2O_2 concentration and bath temperature on morphology, Mater. Sci. Semicond.Process., 2013; 16:1943-1948.
[32] Yousefi T, Nozad GA, Mashhadizadeh MH, Aghazadeh M. Template-free synthesis of MnO_2 nanowires with secondary flower like structure: Characterization and supercapacitor behavior studies, Curr. Appl. Phys. 2012; 12: 193-198.
[33] Yousefi T, Nozad GA, Mashhadizadeh MH. Synthesis of iron oxide nanoparticles at low bath temperature: Characterization and energy storage studies, Mater. Sci. Semicond. Process. 2013; 16: 1837-1841.
[34] Yousefi T, Davarkhah R, Nozad GA, Mashhadizadeh MH. Synthesis, characterization, and supercapacitor studies of manganese (IV) oxide nanowires, Mater. Sci. Semicond. Process, 2013; 16: 868-876.
[35] Li Y, Tan B, Wu Y. Ammonia-evaporation-induced synthetic method for metal (Cu, Zn, Cd, Ni) hydroxide/oxide nanostructures. Chem. Mater, 2008; 20: 567–76.
[36] Liang, Kun-Yu W, Joshua P, Hong-Cai Z. Controllable Synthesis of Metal-Organic Frameworks and Their Hierarchical Assemblies, Matter, 2019; 1: 801–824 .
[37] Lili Ke, Shiqiang Luo, Xiaoxue R, Yongbo Y. Factors influencing the nucleation and crystal growth of solution-processed organic lead halide perovskites: a review, J. Phys. D. 54; 2021: 163001.
[38] Zhang Z, Sun H, Shao X, Li D, Yu H, Han M. Three-dimensionally oriented aggregation of a few hundred nanoparticles into monocrystalline architectures. Adv Mater, 2005; 17: 42–7.

[39] Zhang Q, Zhang K, Xu D, Yang G, Huang H, Nie F, Liu C, Yang, S. CuO nanostructures: Synthesis, characterization,growth mechanisms, fundamental properties, and applications, Prog. Mater. Sci. 2014; 60: 208–337.
[40] Yousefi T, Yavarpour S, Mousavi SH, Mostaedi TM, Davarkhah R, Ghasemi HM. Effective removal of Ce(III) and Pb(II) by new hybrid nano-material: $HnPMo_{12}O_{40}$@ Fe(III)(x)Sn(II)(y)Sn(IV)(1-x-y), Process Saf. Environ. 2015; 98: 211-220.
[41] Yousefi T, Yavarpour S, Mousavi SH, Mostaedi TM, Davarkhah R, Ghasemi HM. $FeIII_xSnII_ySnIV_{1-x-y}H_n[P(Mo_3O_{10})_4]\cdot xH_2O$ new nano hybrid, for effective removal of Sr(II) and Th(IV), J. Radioanal. Nucl. Chem., 2016; 307: 941-953.
[42] Ho YS, McKay G. Pseudo-second order model for sorption processes, Process Biochemistry, 1999; 34: 451–465.
[43] Plazinski W, Dziuba J, Rudzinski W. Modeling of sorption kinetics: the pseudo-second order equation and the sorbate intraparticle diffusivity, Adsorption, 2013; 19(5) :1055–1064.
[44] Sani T, Gómez HL, Pérez PJ, Chebude YDI. Defluoridation performance of nano-hydroxyapatite/stilbite composite compared with bone char, Separation and Purification Technology, 2016;157: 241-248.
[45] Zúñiga MNM, Bonilla PA, Mendoza CDI, Reynel ÁHE, Tapia JCP. Fluoride adsorption properties of cerium-containing bone char, J. Fluorine Chem., 2017; 197: 63-73.
[46] Zhang J, Chen N, Su P, Li M, Feng Ch. Fluoride removal from aqueous solution by Zirconium-Chitosan/Graphene Oxide Membrane, Reactive and Functional Polymers, 2017; 14:127-135.
[47] Biswas K, Saha SK, Ghosh UC. Adsorption of fluoride from aqueous solutionby a synthetic iron(III)–aluminum(III) mixed oxide, Ind. Eng. Chem. Res. 2007; 46: 5346–5356.
[48] Ruan Zh, Tian Y, Ruan J, Cui G, Iqbal K, Iqbal A, Ye H, Yang Zh, Yan Sh. Synthesis of hydroxyapatite/multi-walled carbon nanotubes for the removal of fluoride ions from solution, Applied Surface Science, 2017; 412: 578-590.
[49] Chen S L, Yong Z, Hong H, Jiu X, Jin HH. Enhanced fluoride removal from water by sulfate-doped hydroxyapatite hierarchical hollow microspheres, Chem. Eng. J., 2016; 285:616-624.
[50] Biswas K, Gupta K, Goswami A. Fluoride removal efficiency fromaqueous solution by synthetic iron(III)–aluminum(III)–chromium(III) ternarymixed oxide, Desalination, 2010; 255: 44–51.
[51] Tangsir S, Divband HL, Lähde A, Maljanen M, Hooshmand A, Naseri AA, Moazed H, Jokiniemi J, Bhatnagar A. Water defluoridation using Al_2O_3 nanoparticles synthesized by flame spray pyrolysis (FSP) method, Chem. Eng. J., 2016; 288: 198-206.
[52] Zhang S, Lu Y, Lin X, Su X, Zhang Y. Removal of fluoride from groundwater by adsorption onto La(III)- Al(III) loaded scoria adsorbent, Appl. Surf. Sci. 2014; 303: 1-5.
[53] Chenga J, Meng X, Jing C, Hao J. La^{3+}-modified activated alumina for fluoride removal from water, J. Hazard Mater. 2014; 278: 343–349.
[54] Ghosh A, Chakrabarti S, Biswas K, Chand GU. Agglomerated nanoparticles of hydrous Ce(IV) + Zr(IV) mixed oxide: Preparation, characterization and physicochemical aspects on fluoride adsorption, Appl. Surf. Sci. 2014; 307: 665–676.
[55] Gḿez HL, Pinar AB, Pérez PJ, Sani T, Chebude Y, Isabel D. Ion-exchange in natural zeolite stilbite and significance in defluoridation ability, Micropor. Mesopor. Mat., 2014; 193:93–102.
[56] Gómez HL, Pérez P, Raquel GJ, Chebude Y, Día I. Natural zeolites from Ethiopia for elimination of fluoride from drinking water, Sep. Purif. Technol., 2013; 120: 224-229.
[57] Singh K, Lataye DH, Wasewar KL. Removal of fluoride from aqueous solution by using bael (Aegle marmelos) shell activated carbon: Kinetic, equilibrium and thermodynamic study, J. Fluorine Chem., 2017; 194: 23-32.
[58] Bhaumik R, Mondal NK, Chattoraj S. An optimization study for defluoridation from synthetic Fluoride solution using scale of Indian major carp Catla (Catla catla): An Unconventional Biosorbent, J. Fluorine Chem. 2017; 195: 57–69.
[59] Barathi M, Kumar ASK, Rajesh N. Efficacy of novel Al–Zr impregnated cellulose adsorbent prepared using microwave irradiation for the facile defluoridation of water, J. Environ. Chem. Eng., 2013; 1:1325-1335.
[60] Nazari M, Halladj R. Adsorptive removal of fluoride ions from aqueous solution by using sonochemically synthesized nanomagnesia/alumina adsorbents: An experimental and modeling study, J. Taiwan Institute Chem. Eng. 2014; 65: 2518-2525.
[61] Biswas K, Bandhoyapadhyay D, Ghosh UC. Adsorption kinetics of fluoride oniron(III)–zirconium(IV) hybrid oxide, Adsorption, 2007; 13: 83–94.
[62] Denga Sh, Liu H, Zhou W, Huang J,Yua G. Mn–Ce oxide as a high-capacity adsorbent for fluoride removal from water, J. Hazard. Mater. 2011; 186:1360–1366.
[63] Paudyal H, Pangeni B, Inoue K. Adsorptive removal of fluoride fromaqueous solution using orange waste loaded with multi-valent metal ions, J. Hazard. Mater. 2011; 192:676–682.
[64] Freundlich H. Over the Adsorption in Solution J. Phys. Chem. A., 1906; 57: 385-471.
[65] Dada A, Olalekan A, Olatunya A, Dada O. Langmuir, Freundlich. Temkin and Dubinin–Radushkevich isotherms studies of equilibrium sorption of Zn^{2+} unto phosphoric acid modified rice husk, J. Appl. Chem. 2012; 3:38-45.
[66] Vijayaraghavan K, Padmesh T, Palanivelu K, Velan M. Biosorption of nickel(II) ions onto Sargassum wightii: application of two-parameter and three-parameter isotherm models, J. Hazard. Mater. 2006; 133: 304-308.